Neuron, Volume *82*

Supplemental Information

Miniature Neurotransmission Regulates *Drosophila* Synaptic Structural Maturation

Ben Jiwon Choi, Wendy L. Imlach, Wei Jiao, Verena Wolfram, Ying Wu, Mark Grbic, Carolina Cela, Richard A. Baines, Michael N. Nitabach, and Brian D. McCabe

Abbreviation	Genotype	N #	Control	Synaptic Terminal Area (μm^2) (Significance vs Control)	Number of typical synaptic bouton (number) (Significance vs Control)	Number of small synaptic bouton (number) (Significance vs Control)	Bouton size index (number) (Significance vs Control)
Control(toxin) CS	CantonS	48	**N/A**	292.4±7.976	24.000±0.672	2.878±0.301	0.1254±0.0146
UAS-TeTxLC	UAS-TeTxLC/*OK319-Gal4*	54	**CS**	300.09±8.574 (ns)	24.056±0.690 (ns)	3.333±0.400 (ns)	0.1511±0.0205 (ns)
UAS-PLTXII	*OK6- Gal4/+;+/UAS-PLTXII*	39	**CS**	301.84±7.674 (ns)	23.556±0.537 (ns)	2.143±0.229 (ns)	0.0921±0.0111 (ns)
Control(*vglut*) *vglut*$^{Df/+}$	*Vglut*$^{OK371\Delta D}$/+	37	**N/A**	347.79±8.283	34.162±0.857	4.000±0.365	0.1215±0.0125
***vglut*^{MN}**	*vglut*^{1}/*vglut*$^{OK371\Delta D}$,*UAS-Vglut-RNAi*^{JF02689};*D42-Gal4/UAS-Vglut-RNAi*^{VDRC104324}	30	***vglut*$^{Df/+}$**	263.02±8.734 (***)	22.967±0.702 (***)	9.433±0.974 (***)	0.4447±0.0543 (***)
Vglut-RNAi#1	*UAS-Vglut-RNAi*^{VDRC104324}/+; *UAS-Vglut-RNAi*^{JF02689}/*D42-Gal4*	33	**CS**	271.09±4.996 (*)	21.879±0.701 (*)	5.827±0.665 (***)	0.2508±0.0340 (**)
Vglut-RNAi#2	*OK6-Gal4/+;D42-Gal4/UAS-Vglut-RNAi*^{HMS02011}	32	**CS**	263.65±8.578 (*)	20.000±0.743 (***)	6.281±0.570 (***)	0.3426±0.0382 (***)
***vglut*^{Hypo}**	*vglut*^{1}/*vglut*$^{OK371\Delta D}$	48	***vglut*$^{Df/+}$**	302.21±4.204 (***)	27.021±0.633 (***)	6.292±0.478 (**)	0.2368±0.0182 (***)
***vglut*^{Hypo} + UAS-Vglut**	*vglut*^{1},*OK319-Gal4/vglut*$^{OK371\Delta D}$;*+/UAS-Vglut*	24	***vglut*$^{Df/+}$**	359.34±20.947 (ns)	30.435±1.002 (**)	3.150±0.399 (ns)	0.0905±0.0134 (ns)
Control (Fig.2) *dgluRIIA*$^{+/-}$,*IIB*$^{Df/-}$	*dglurIIA,IIB*^{sp22}/ *Df(2L)cl*^{h4} ; *genomic-dglurIIA/+*	44	**N/A**	302.83±6.05	32.886±0.927	2.136±0.267	0.06784±0.0091
***dgluRIIA*$^{Hypo/-}$,*IIB*$^{Df/-}$**	*dglurIIA,IIB*^{sp22}/ *Df(2L)cl*^{h4}, *genomic-dglurIIAΔ3UTR*						
***iGluR*^{WT}**	*dglurIIA,IIB*^{sp22}/ *Df(2L)cl*^{h4}, *genomic-dglurIIA*Δ3UTR; *genomic-dglurIIA*^{WT}/+	59	***dgluRIIA*$^{+/-}$,*IIB*$^{Df/-}$**	318.25±6.910 (ns)	30.862±0.683 (ns)	2.259±0.253 (ns)	0.07391±0.00864 (ns)
***iGluR*^{MUT}**	*dglurIIA,IIB*^{sp22}/ *Df(2L)cl*^{h4}, *genomic-dglurIIA*Δ3UTR; *genomic-dglurIIA*^{E783A}/+	53	***dgluRIIA*$^{+/-}$,*IIB*$^{Df/-}$ (Fig. 2) *iGluR*^{WT} (Fig. 3,5,7,8)**	231.12±7.906 (***)	19.850±0.843 (***)	6.025±0.541 (***)	0.3272±0.0330 (***)
***iGluR*^{MUT} + UAS-dGluR^{WT}**	*dglurIIA,IIB*^{sp22},*G14-Gal4/ Df(2L)cl*^{h4}, *genomic-dglurIIA*Δ3UTR; *genomic-dglurIIA*^{E783A}/*UAS-dglurIIA*	22	***dgluRIIA*$^{+/-}$,*IIB*$^{Df/-}$**	345.16±11.512 (***)	27.773±0.822 (**)	3.421±0.650 (ns)	0.1161±0.0298 (ns)
***iGluR*^{MUT} + UAS-CamKII^{Act}**	*dglurIIA,IIB*^{sp22},*G14-Gal4/ Df(2L)cl*^{h4}, *genomic-dglurIIA*Δ3UTR; *genomic-dglurIIA*^{E783A}/*UAS-CamKII*^{T287D}	17	***iGluR*^{WT}**	260.65±14.480 (**)	22.824±0.892 (***)	9.823±0.792 (***)	0.4483±0.0473 (***)
***iGluR*^{MUT} + UAS-CamKII^{Inh}**	*dglurIIA,IIB*^{sp22},*G14-Gal4/ Df(2L)cl*^{h4}, *genomic-dglurIIA*Δ3UTR; *genomic-dglurIIA*^{E783A}/*UAS-CamKIINtide*	19	***iGluR*^{WT}**	260.64±10.837 (***)	20.842±0.922 (***)	8.684±0.722 (***)	0.4377±0.0415 (***)
***iGluR*^{MUT} + UAS-PLTXII**	*dglurIIA,IIB*^{sp22},*OK319-Gal4/ Df(2L)cl*^{h4}, *genomic-dglurIIA*Δ3UTR; *genomic-dglurIIA*^{E783A}/*UAS-PLTXII*	36	***iGluR*^{WT}**	240.60±10.122 (***)	20.721±0.661 (***)	6.932±0.505 (***)	0.3276±0.0252 (***)
***iGluR*^{MUT} + UAS-δACTX**	*dglurIIA,IIB*^{sp22},*OK319-Gal4/ Df(2L)cl*^{h4}, *genomic-dglurIIA*Δ3UTR; *genomic-dglurIIA*^{E783A}/ *UAS-δACTX*	27	***iGluR*^{WT}**	252.36±14.182 (***)	21.96±1.194 (***)	6.231±0.939 (***)	0.2819±0.0423 (***)
***iGluR*^{MUT} + UAS-rGluK2**	*dglurIIA,B*^{sp22},*G14-Gal4/ Df(2L)cl*^{h4}, *genomic-dglurIIA*Δ3UTR; *genomic-dglurIIA*^{E783A}/ *UAS-rGluK2*	41	***iGluR*^{WT}**	331.91±6.168 (ns)	27.780±0.693 (**)	4.268±0.446 (***)	0.1553±0.01610 (***)
***iGluR*^{MUT} + UAS-rGluK2 + UAS-PLTXII**	*dglurIIA,IIB*^{sp22},*G14-Gal4,OK319-Gal4/ Df(2L)cl*^{h4}, *genomic-dglurIIA*Δ3UTR; *genomic-dglurIIA*^{E783A},*UAS-PLTXII/UAS-rGluK2*	34	***iGluR*^{WT}**	318.95±9.954 (ns)	27.647±0.736 (**)	4.206±0.372 (***)	0.1568±0.01447 (***)
UAS-PLTXII (muscle)	*G14-Gal4/+;+/UAS-PLTXII*	15	**CS**	305.66±15.387 (ns)	26.667±1.120 (ns)	4.142±0.592 (*)	0.1505±0.02657 (ns)

Table S1

UAS-rGluK2 (neuron)	*OK319-Gal4/+;+/UAS-rGluK2*	16	**CS**	308.34±13.395 (ns)	24.125±0.645 (ns)	2.231±0.441 (ns)	0.07540±0.01777 (ns)
***vglut*^{Hypo} + UAS-PLTXII**	*vglut*^{1},*OK319-Gal4/vglut* $^{OK371\Delta D}$*;+/UAS-PLTXII*	26	***vglut*$^{Df/+}$**	298.85±7.872 (***)	25.308±0.658 (***)	6.731±0.890 (*)	0.2825±0.04470 (***)
***vglut*^{Hypo} + UAS-δACTX**	*vglut*^{1},*OK319-Gal4/vglut* $^{OK371\Delta D}$*;+/UAS- δACTX*	25	***vglut*$^{Df/+}$**	288.72±13.379 (**)	25.520±1.022 (***)	6.760±0.710 (**)	0.2705±0.03107 (***)
Control(*cpx*) *cpx*$^{Df/+}$	*Df(3R)ED5021/+*	35	**N/A**	282.98±6.927	25.694±0.720	3.556±0.426	0.1407±0.0163
***cpx*$^{-/-}$**	*Df(3R)ED5021/cpx*^{SH1}	38	***cpx*$^{Df/+}$**	407.96±11.755 (***)	33.795±1.068 (***)	1.897±0.276 (**)	0.0598±0.00902 (***)
***cpx*$^{-/-}$ + UAS-Cpx**	*UAS-Cpx/+;OK6-Gal4/+;Df(3R)ED5021/cpx*^{SH1}	46	***cpx*$^{Df/+}$**	312.79±8.318 (ns)	28.067±0.853 (ns)	4.933±0.433 (*)	0.1863±0.0172 (ns)
***Cpx*$^{1257/-}$**	*Df(3R)ED5021/cpx*^{1257}	23	***cpx*$^{Df/+}$**	432.33±26.326 (***)	33.65±0.8331 (***)	3.182±0.439 (ns)	0.08891±0.0136 (*)
***cpx*$^{-/-}$ + UAS-PLTXII**	*OK6-Gal4/UAS-PLTXII;Df(3R)ED5021/cpx*^{SH1}	24	***cpx*$^{Df/+}$**	391.62±10.172 (***)	35.50±1.234 (***)	1.292±0.321 (***)	0.03705±0.00896 (***)
***cpx*$^{-/-}$ + UAS-dGluR^{DN}**	*G14-Gal4/UAS-dglurIIA*^{E783A}*;Df(3R)ED5021/ cpx*^{SH1}	41	***cpx*$^{Df/+}$**	262.65±10.146 (ns)	25.105±0.951 (ns)	3.447±0.507 (ns)	0.1518±0.0289 (ns)
***cpx*$^{-/-}$ + Vglut-RNAi**	*OK6-Gal4/ UAS-Vglut-RNAi*^{VDRC104324}*;Df(3R)ED5021 /cpx*^{SH1}	56	***cpx*$^{Df/+}$**	333.78±7.394 (**)	28.585±0.839 (ns)	5.018±0.455 (*)	0.1881±0.0193 (*)
UAS-dGluR^{DN}	*G14-Gal4/UAS-dglurIIA*^{E783A}	29	**CS**	279.49±10.734 (ns)	25.964±0.864 (ns)	2.071±0.329 (*)	0.08391±0.0138 (*)
Vglut-RNAi	*OK6-Gal4/ UAS-Vglut-RNAi*^{VDRC104324}	28	**CS**	275.59±9.57 (ns)	26.034±1.318 (ns)	5.241±0.683 (***)	0.2152±0.0327 (***)
***trio*$^{-/-}$**	*trio*^{S137203}*/trio*^{S137203}	30	**CS**	192.81±8.794 (***)	17.194±0.905 (***)	5.700±0.526 (***)	0.3549±0.4404 (***)
***Trio*$^{-/-}$ + UAS-Trio**	*UAS-Trio/+;+/OK319-Gal4; trio*^{S137203}*/trio*^{S137203}	23	**CS**	291.98±12.734 (ns)	23.608±0.963 (ns)	2.545±0.3821 (ns)	0.09846±0.01471 (ns)
***trio*$^{-/-}$; *cpx*$^{-/-}$**	*trio*^{S137203}*/trio*^{S137203}*; cpx*^{SH1}*/cpx*^{SH1}	28	***cpx*$^{Df/+}$**	204.62±8.34 (***)	19.467±0.716 (***)	7.267±0.959 (**)	0.3893±0.0524 (***)
***iGluR*^{MUT} + UAS-Trio**	*dglurIIA,IIB*^{sp22}*,OK319-Gal4/ Df(2L)cl*^{h4}*, genomic-dglurIA*Δ3UTR*; genomic-dglurIA*^{E783A}*/UAS-Trio*	30	***iGluR*^{WT}**	305.37±14.7 (ns)	28.74±1.07 (ns)	5.345±0.659 (***)	0.1842±0.0253 (***)
***iGluR*^{MUT} + UAS-Rac1^{WT}**	*dglurIIA,IIB*^{sp22}*,OK319-Gal4/ Df(2L)cl*^{h4}*, genomic-dglurIA*Δ3UTR*; genomic-dglurIA*^{E783A}*/UAS-Rac1*	23	***iGluR*^{WT}**	256.03±16.41 (**)	22.09±1.17 (***)	5.909±0.916 (***)	0.3478±0.0620 (***)
***iGluR*^{MUT} + UAS-Rac1^{Act}**	*dglurIIA,IIB*^{sp22}*,OK319-Gal4/ Df(2L)cl*^{h4}*, genomic-dglurIA*Δ3UTR*; genomic-dglurIA*^{E783A}*/UAS-Rac1*^{V12}	23	***iGluR*^{WT}**	306.46±19.93 (ns)	30.2±0.846 (ns)	5.077±0.604 (***)	0.1482±0.0226 (**)
***iGluR*^{WT} + *trio*$^{-/-}$**	*dglurIIA,IIB*^{sp22}*/ Df(2L)cl*^{h4}*, genomic-dglurIA*Δ3UTR*; trio*^{S137203}*,genomic-dglurIA/ trio*^{S137203}	35	***iGluR*^{WT}**	180.53±7.62 (***)	11.861±0.524 (***)	4.297±0.525 (***)	0.4459±0.0814 (***)
***iGluR*^{MUT} + *trio*$^{-/-}$**	*dglurIIA,IIB*^{sp22}*/ Df(2L)cl*^{h4}*, genomic-dglurIA*Δ3UTR*; trio*^{S137203}*,genomic-dglurIA*^{E783A}*/ trio*^{S137203}	24	***iGluR*^{WT}**	188.25±7.93 (***)	13.125±0.588 (***)	6.960±0.488 (***)	0.5243±0.0343 (***)
***iGluR*^{WT} + UAS-Trio**	*dglurIIA,IIB*^{sp22}*,OK319-Gal4/ Df(2L)cl*^{h4}*, genomic-dglurIA*Δ3UTR*; genomic-dglurIA*^{WT}*/UAS-Trio*	26	***iGluR*^{WT}**	347.17±8.94 (*)	33.96±0.774 (**)	3.038±0.316 (ns)	0.089±0.01046 (ns)
***iGluR*^{WT} + UAS-Rac1^{WT}**	*dglurIIA,IIB*^{sp22}*,OK319-Gal4/ Df(2L)cl*^{h4}*, genomic-dglurIA*Δ3UTR*; genomic-dglurIA*^{WT}*/UAS-Rac1*^{WT}	32	***iGluR*^{WT}**	380.60±14.53 (***)	35.43±1.04 (***)	8.100±0.894 (***)	0.2301±0.02714 (***)
***iGluR*^{WT} + UAS-Rac1^{Act}**	*dglurIIA,IIB*^{sp22}*,OK319-Gal4/ Df(2L)cl*^{h4}*, genomic-dglurIA*Δ3UTR*; genomic-dglurIA*^{WT}*/UAS-Rac1*^{V12}	22	***iGluR*^{WT}**	316.51±12.74 (ns)	31.08±1.16 (ns)	4.208±0.430 (***)	0.1355±0.01251 (***)

Table S1 (Continued)

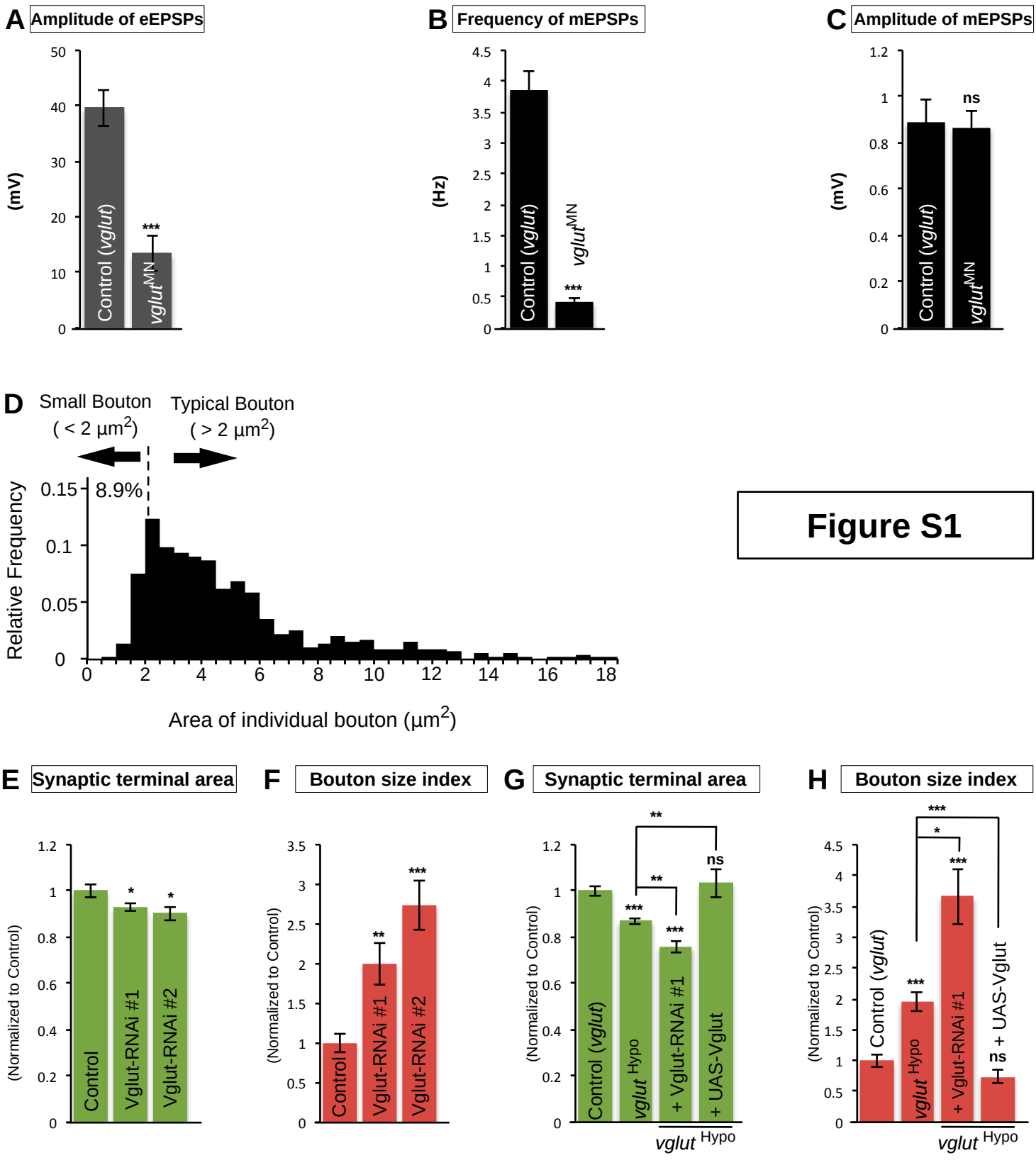

Figure S1

vglut MN = *vglut* Hypo + Vglut-RNAi #1

Figure S1. Electrophysiological and morphological quantification of *vglut* mutants and bouton size distribution of wild type terminals, Related to Figure 1.

A-C, Quantification of (A) the amplitude of eEPSPs (n≥6), (B) the frequency of mEPSPs and (C) the amplitude of mEPSPs (n≥9). **D,** Relative frequency histogram for the distribution of individual bouton sizes of wild type (CS) boutons in 0.5μm^2 increments. (n=603 boutons from n=16 NMJs) **E-H**, Quantification of the NMJ (E,G) synaptic terminal area and (F,H) bouton size index (n≥24) of the **Control** [CS], **Vglut1-RNAi#1** [*+/UAS-Vglut-RNAi*^{KK}*;D42-Gal4/UAS-Vglut-RNAi*^{JF}], **Vglut1-RNAi#2** [*OK6-Gal4/+;D42-Gal4/UAS-Vglut-RNAi*^{HMS}], **Control(*vglut*)** [*vglut*$^{Df/+}$], ***vglut*^{Hypo}** [*vglut*$^{Hypo/Df}$], ***vglut*^{Hypo} + Vglut-RNAi#1** [***vglut*^{MN}** = *vglut*$^{Hypo/Df}$,*UAS-Vglut-RNAi*^{KK}*;D42-Gal4/UAS-Vglut-RNAi* ^{JF}] and ***vglut*^{Hypo} + UAS-Vglut** [*vglut*$^{Hypo/Df}$,*OK319-Gal4;+/UAS-Vglut*] normalized to controls [CS for E,F and *vglut*$^{Df/+}$ for G,H] Error bars indicate ± s.e.m. *=p<0.05, **= p<0.01, ***=p< 0.001.

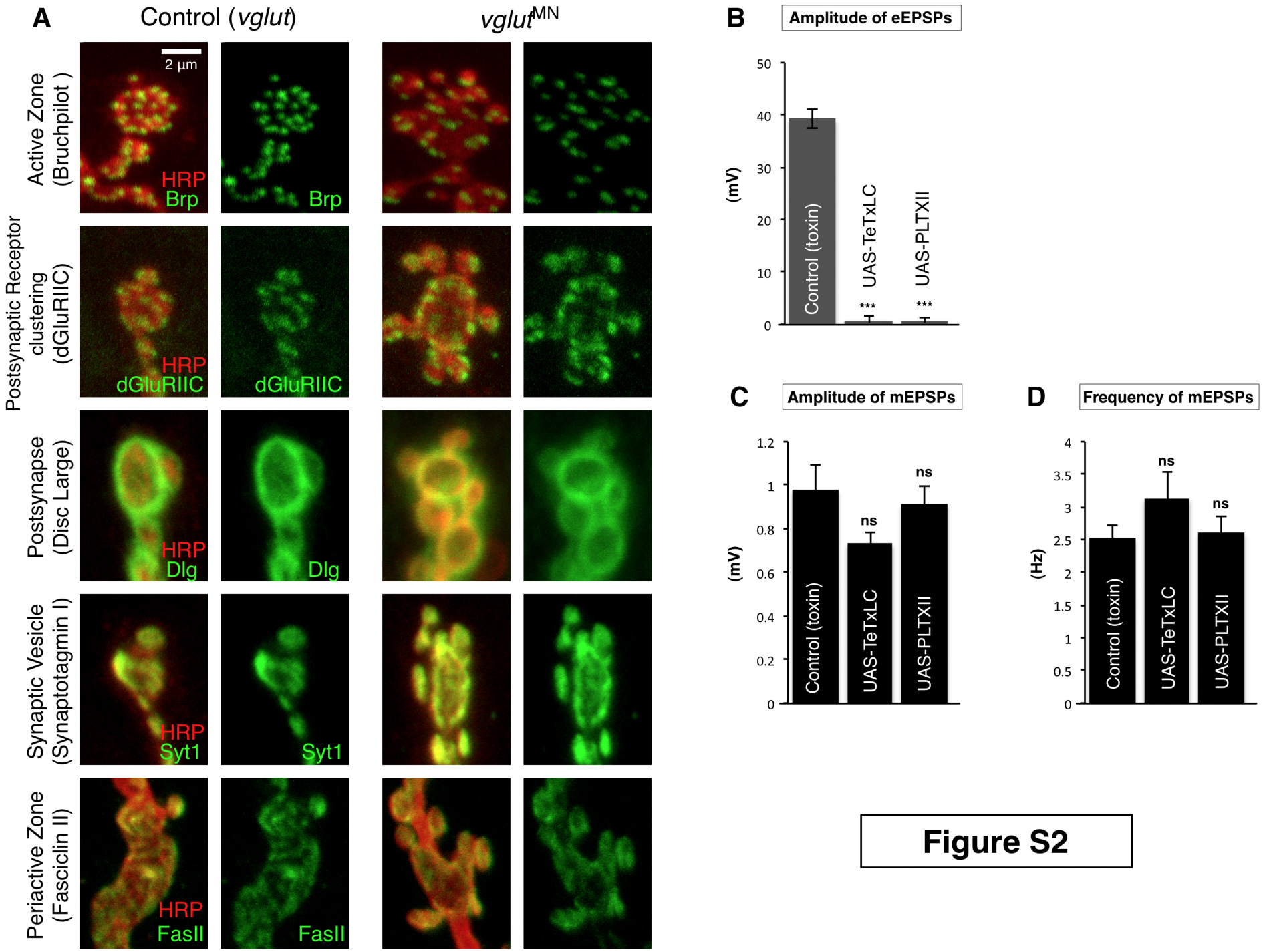
A
Control (vglut)
vglutMN
2 µm
Active Zone (Bruchpilot)
HRP Brp
Brp
Postsynaptic Receptor clustering (dGluRIIC)
HRP dGluRIIC
dGluRIIC
Postsynapse (Disc Large)
HRP Dlg
Dlg
Synaptic Vesicle (Synaptotagmin I)
HRP Syt1
Syt1
Periactive Zone (Fasciclin II)
HRP FasII
FasII
B
Amplitude of eEPSPs
(mV)
50
40
30
20
10
0
Control (toxin)
UAS-TeTxLC
UAS-PLTXII
***
***
C
Amplitude of mEPSPs
(mV)
1.2
1
0.8
0.6
0.4
0.2
0
Control (toxin)
UAS-TeTxLC
UAS-PLTXII
ns
ns
D
Frequency of mEPSPs
(Hz)
4
3.5
3
2.5
2
1.5
1
0.5
0
Control (toxin)
UAS-TeTxLC
UAS-PLTXII
ns
ns

Figure S2

Figure S2. Synaptic markers at small boutons of *vglut* mutants and electrophysiological quantification of toxin mutants, Related to Figure 1.

A, Representative boutons from control(*vglut*) [$vglut^{Df/+}$] and $vglut^{MN}$ at muscle 4 labeled with indicated synaptic markers (green) and the neuronal membrane marker HRP (red). Scale is the same for all images. **B-D**, Quantification of (B) the amplitude of eEPSPs ($n \geq 6$), (C) the amplitude of mEPSPs and (D) the frequency of mEPSPs ($n \geq 9$). All error bars indicate ± s.e.m. * =$p<0.05$, ***=$p< 0.001$.

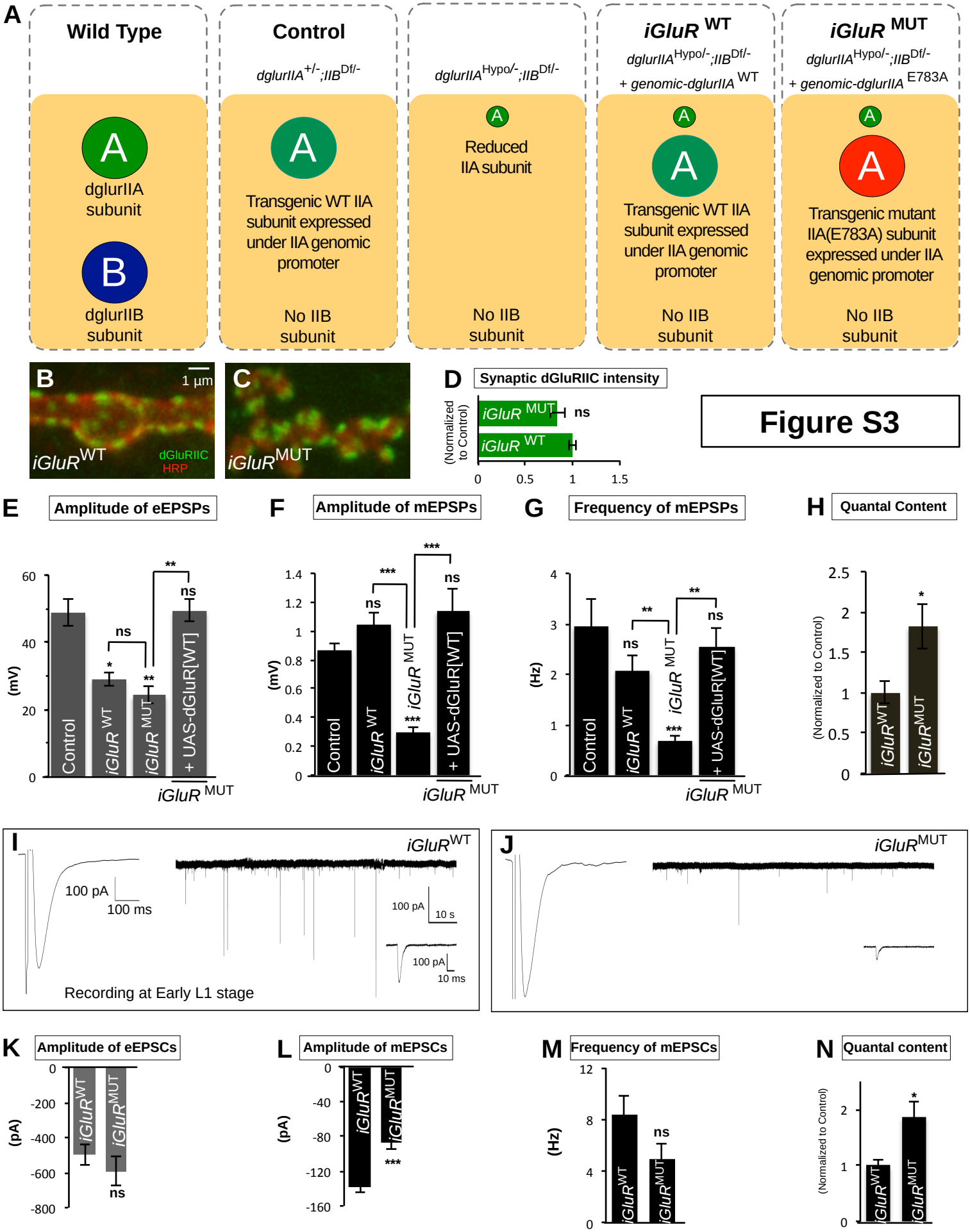
A
Wild Type
dglurIIA subunit
B
dglurIIB subunit
Control
dglurIIA+/-;IIBDf/-
A
Transgenic WT IIA subunit expressed under IIA genomic promoter
No IIB subunit
dglurIIAHypo/-;IIBDf/-
A
Reduced IIA subunit
No IIB subunit
iGluR WT
dglurIIAHypo/-;IIBDf/-
+ genomic-dglurIIA WT
A
A
Transgenic WT IIA subunit expressed under IIA genomic promoter
No IIB subunit
iGluR MUT
dglurIIAHypo/-;IIBDf/-
+ genomic-dglurIIA E783A
A
A
Transgenic mutant IIA(E783A) subunit expressed under IIA genomic promoter
No IIB subunit
B
1 µm
iGluRWT
dGluRIIC
HRP
C
iGluRMUT
D
Synaptic dGluRIIC intensity
(Normalized to Control)
iGluR MUT
ns
iGluR WT
0
0.5
1
1.5
Figure S3
E
Amplitude of eEPSPs
(mV)
60
40
20
0
Control
iGluR WT
iGluR MUT
+ UAS-dGluR[WT]
iGluR MUT
*
**
ns
**
ns
F
Amplitude of mEPSPs
(mV)
1.4
1.2
1
0.8
0.6
0.4
0.2
0
Control
iGluR WT
iGluR MUT
+ UAS-dGluR[WT]
iGluR MUT
***
ns
***
***
ns
G
Frequency of mEPSPs
(Hz)
4
3
2
1
0
Control
iGluR WT
iGluR MUT
+ UAS-dGluR[WT]
iGluR MUT
**
ns
**
***
ns
H
Quantal Content
(Normalized to Control)
2.5
2
1.5
1
0.5
0
iGluRWT
iGluRMUT
*
I
iGluRWT
100 pA
100 ms
100 pA
10 s
100 pA
10 ms
Recording at Early L1 stage
J
iGluRMUT
K
Amplitude of eEPSCs
(pA)
0
-200
-400
-600
-800
iGluRWT
iGluRMUT
ns
L
Amplitude of mEPSCs
(pA)
0
-40
-80
-120
-160
iGluRWT
iGluRMUT
***
M
Frequency of mEPSCs
(Hz)
12
8
4
0
iGluRWT
iGluRMUT
ns
N
Quantal content
(Normalized to Control)
2
1
0
iGluRWT
iGluRMUT
*

Figure S3. iGluR mutant genotypes, abbreviations, synaptic receptor levels, quantification of electrophysiology, Related to Figure 2.

A, Schematic of abbreviations, genotype, subunit composition and description of iGluR mutants in Figure 2. **B,C**, Representative terminals from (B) *iGluR*^{WT} and (C) *iGluR*^{MUT}, labeled with the iGluR subunit, dGluRIIC (green) and the neuronal membrane marker HRP (red). dGluRIIC is an obligatory co-subunit required for functional channels with dGluRIIA. iGluR synaptic clustering is similar in *iGluR*^{WT} and *iGluR*^{MUT}. **D**, Quantification of the ratio of synaptic dGluRIIC intensity to HRP normalized to control ($n \geq 10$). **E-H**, Quantification of (E) the amplitude of eEPSPs, (F) the amplitude of mEPSPs, (G) the frequency of mEPSPs and (H) normalized quantal content (eEPSP amplitude / mEPSP amplitude after correction for nonlinear summation errors) to control ($n \geq 8$) of the indicated genotypes. **I,J**, Representative traces of excitatory post-synaptic current (eEPSC) (left) and miniature excitatory post-synaptic currents (mEPSCs) (right) recorded from early first instar larvae from *iGluR*^{WT} and *iGluR*^{MUT}. **K-N**, Quantification of (K) the amplitude of eEPSCs, (L) the amplitude of mEPSCs, (M) the frequency of mEPSCs and (N) normalized quantal contents (eEPSC amplitude / mEPSC amplitude) to control ($n \geq 5$) of *iGluR*^{WT} and *iGluR*^{MUT}. Scale is the same between images B,C and between I,J. All error bars indicate ± s.e.m. * =$p<0.05$, ***<0.001.

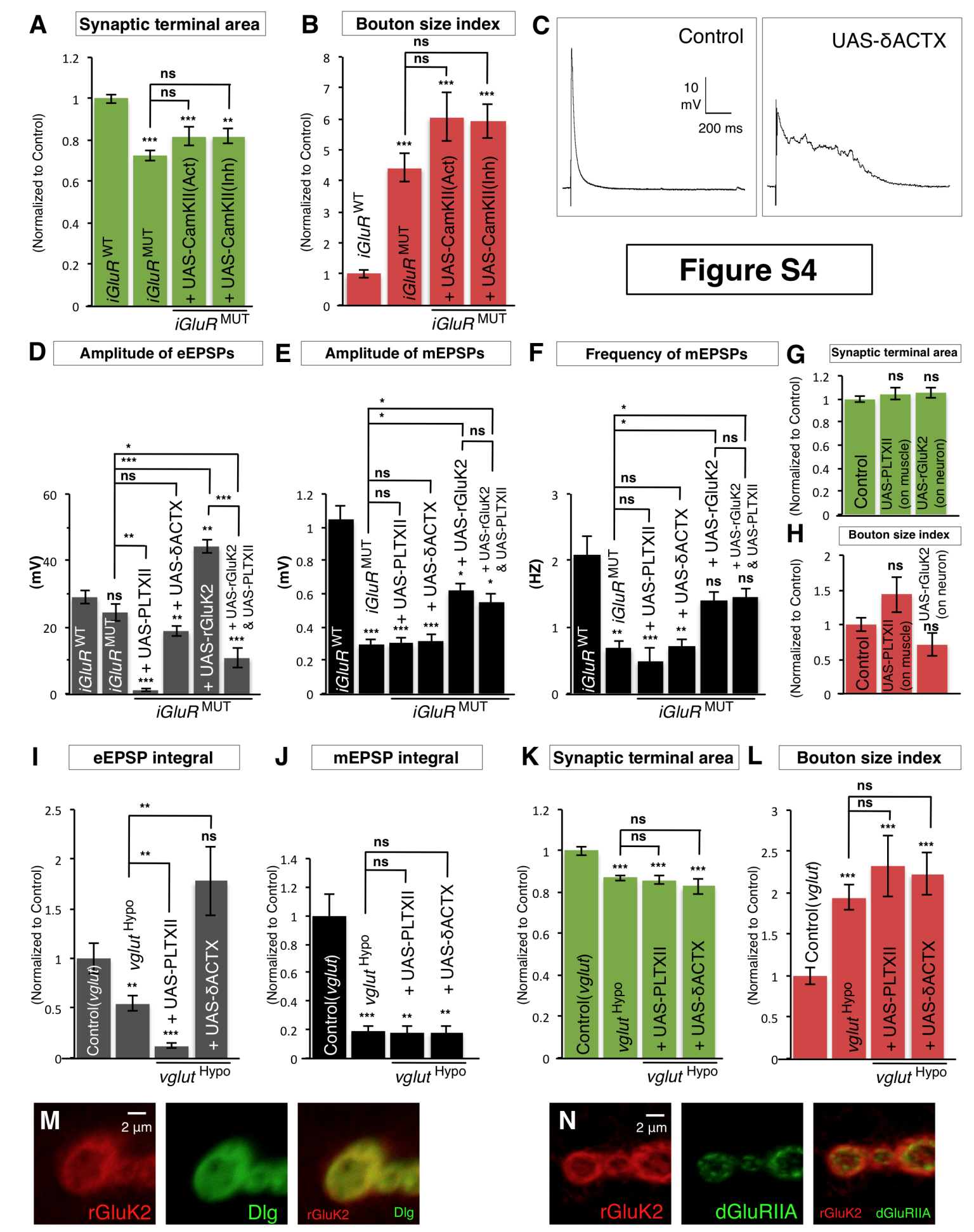
A
Synaptic terminal area
(Normalized to Control)
iGluR WT
iGluR MUT
+ UAS-CamKII(Act)
+ UAS-CamKII(Inh)
iGluR MUT
B
Bouton size index
C
Control
UAS-δACTX
10 mV
200 ms
Figure S4
D
Amplitude of eEPSPs
(mV)
+ UAS-PLTXII
+ UAS-δACTX
+ UAS-rGluK2
+ UAS-rGluK2 & UAS-PLTXII
E
Amplitude of mEPSPs
F
Frequency of mEPSPs
(HZ)
G
Synaptic terminal area
Control
UAS-PLTXII (on muscle)
UAS-rGluK2 (on neuron)
H
Bouton size index
I
eEPSP integral
Control(vglut)
vglut Hypo
vglut Hypo
J
mEPSP integral
K
Synaptic terminal area
L
Bouton size index
M
2 µm
rGluK2
Dlg
rGluK2 Dlg
N
2 µm
rGluK2
dGluRIIA
rGluK2 dGluRIIA

Figure S4. Electrophysiological and morphological quantification and synaptic receptor localization, Related to Figure 2 and Figure 3.

A,B,D-L, Quantification of the NMJ (A,G,K) synaptic terminal area, (B,H,L) bouton size index ($n \geq 17$ for A,B, $n \geq 15$ for G,H and $n \geq 25$ for K,L), (D) the amplitude of eEPSPs, (E) the amplitude of mEPSPs ,(F) the frequency of mEPSPs ($n \geq 8$), (I) eEPSP integral and (J) mEPSP integral ($n \geq 5$) of the indicated genotypes normalized to controls [*iGluR*^{WT} for A,B,D-F, *vglut*$^{Df/+}$ for I-L and CS for G,H]. Detailed description of used genotypes are as follows, ***iGluR*^{MUT}+UAS-CamKII^{Act}** [*dglurIIA*$^{Hypo/-}$*,IIB*$^{Df/-}$*,G14-Gal4;UAS-CamKII*^{T287D}*/genomic-dglurIIA*^{E783A}], ***iGluR*^{MUT}+UAS-CamKII^{Inh}** [*dglurIIA*$^{Hypo/-}$*,IIB*$^{Df/-}$*,G14-Gal4;UAS-CamKIINtide/genomic-dglurIIA*^{E783A}], **Control(*vglut*)** [*vglut*$^{Df/+}$], ***vglut*^{Hypo}**[*vglut*$^{Hypo/Df}$], ***vglut*^{Hypo} + UAS-PLTXII** [*vglut*$^{Hypo/Df}$,*OK319-Gal4;+/UAS-PLTXII*], ***vglut*^{Hypo} + UAS-δACTX** [*vglut*$^{Hypo/Df}$,*OK319-Gal4;+/UAS-δACTX*], **Control** [CS], **UAS-PLTXII (on muscle)** [*G14-Gal4/+;+/UAS-PLTXII*] and **UAS-rGluK2 (on neuron)** [*OK319-Gal4/+;+/UAS-rGluK2*]. **C,** Representative trace of **Control** [CS] and **UAS-δACTX** [*OK319-Gal4/+;+/UAS-δACTX*] **M,N**, Representative terminals from UAS-rGluK2 [*UAS-rGluK2/C57-Gal4*], labled with the rGluK2 (red), Dlg (green for M) or dGluRIIA (green for N). Error bars indicate ± s.e.m. *=$p<0.05$, **= $p<0.01$, ***=$p< 0.001$.

Figure S5

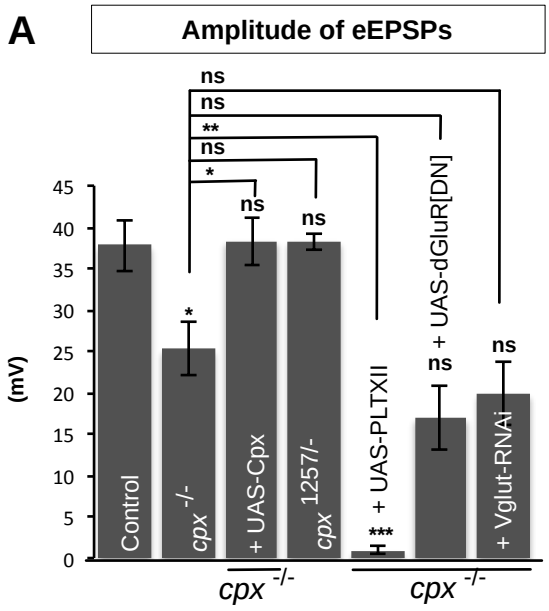
A
Amplitude of eEPSPs
(mV)
Control
cpx -/-
+ UAS-Cpx
1257/- cpx
+ UAS-PLTXII
+ UAS-dGluR[DN]
+ Vglut-RNAi
cpx -/-
cpx -/-

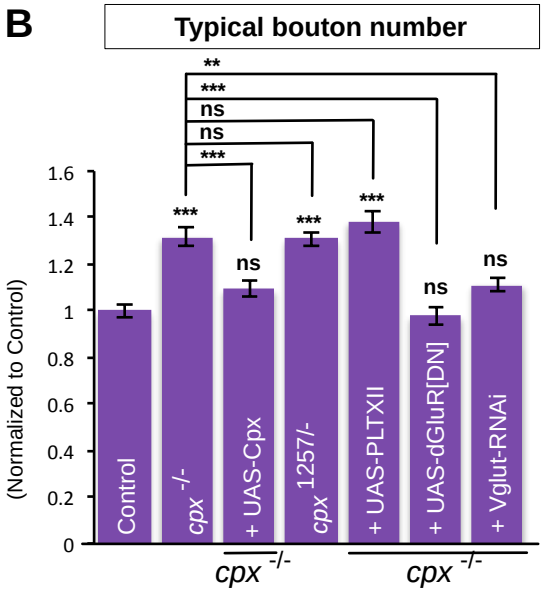
B
Typical bouton number
(Normalized to Control)
Control
cpx -/-
+ UAS-Cpx
1257/- cpx
+ UAS-PLTXII
+ UAS-dGluR[DN]
+ Vglut-RNAi
cpx -/-
cpx -/-

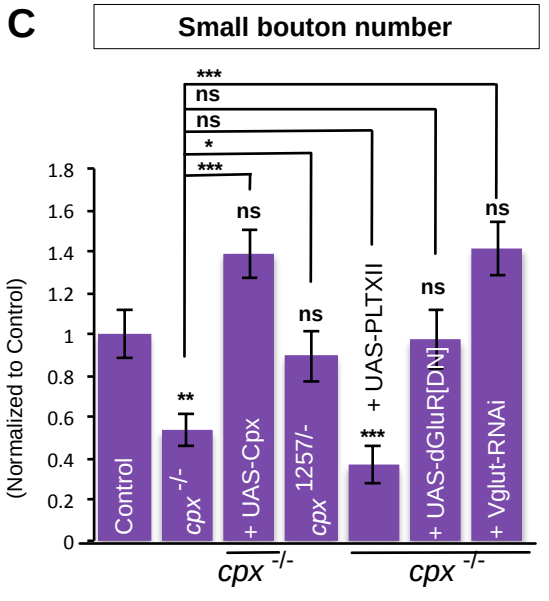
C
Small bouton number
(Normalized to Control)
Control
cpx -/-
+ UAS-Cpx
1257/- cpx
+ UAS-PLTXII
+ UAS-dGluR[DN]
+ Vglut-RNAi
cpx -/-
cpx -/-

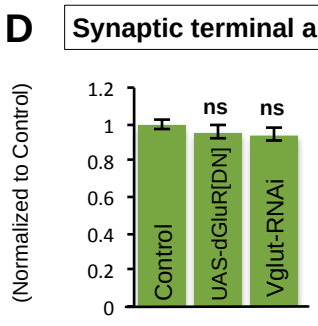
D
Synaptic terminal area
(Normalized to Control)
Control
UAS-dGluR[DN]
Vglut-RNAi

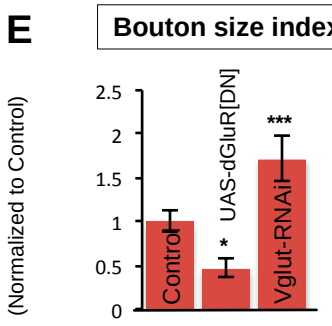
E
Bouton size index
(Normalized to Control)
Control
UAS-dGluR[DN]
Vglut-RNAi

Figure S5. Electrophysiological and morphological quantification of *cpx* mutants, Related to Figure 4.

A-D, Quantification of NMJ (A) the amplitude of eEPSPs (n≥8), (B) typical bouton number, (C) small bouton number (n≥35), (D) synaptic terminal area and (E) bouton size index (n≥28) of the indicated genotypes normalized to controls [*cpx* $^{Df/+}$ for B,C and CS for D,E]. Detailed description of used genotypes are followed, **UAS-dGluR^{DN}** [*G14-Gal4/+;+/UAS-dglurIIA*^{E783A}] and **Vglut-RNAi** [*OK6-Gal4/UAS-Vglut-RNAi*^{KK}]. All error bars indicate ± s.e.m. * =p<0.05, **= p<0.01, ***=p< 0.001.

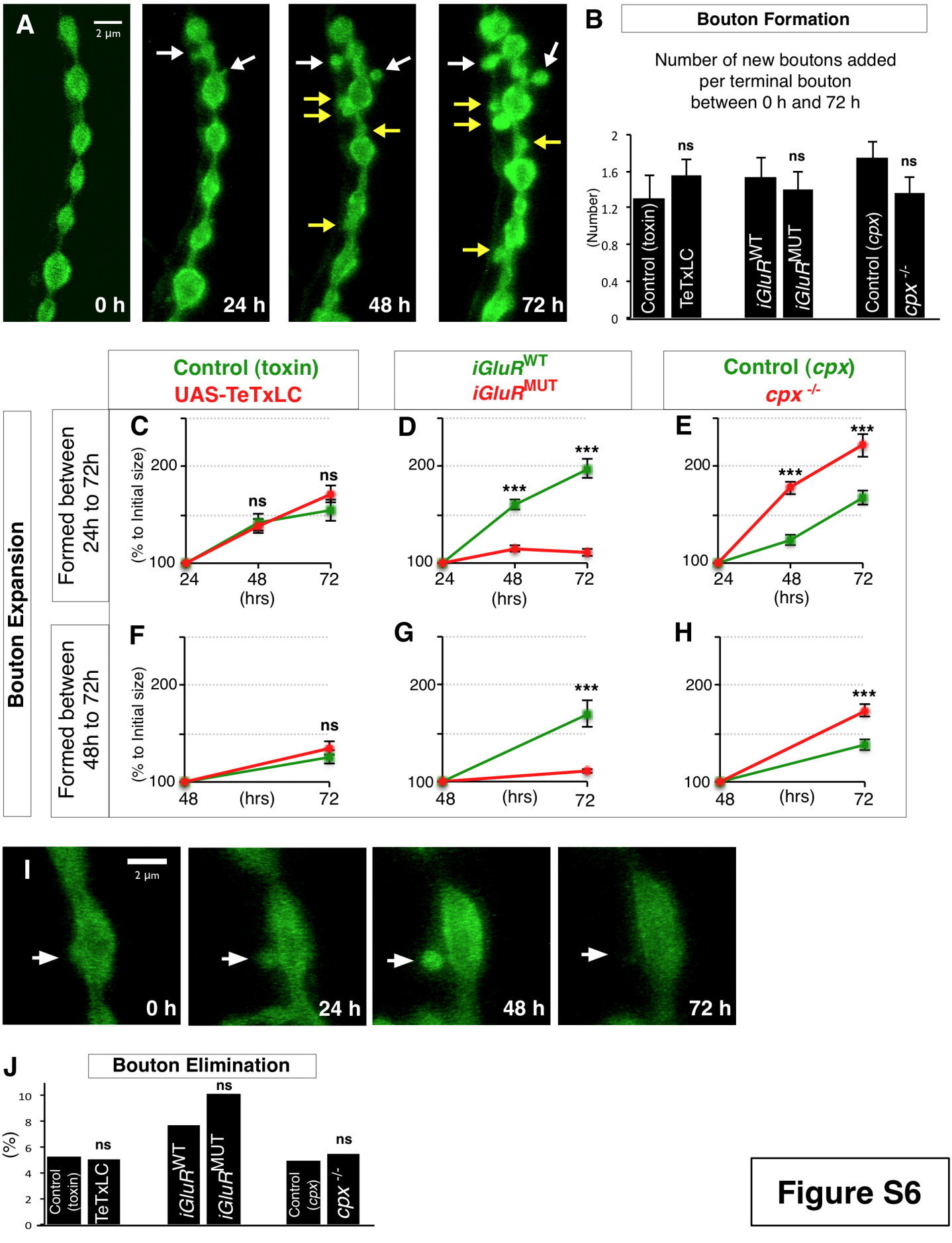
A
2 µm
0 h
24 h
48 h
72 h
B
Bouton Formation
Number of new boutons added per terminal bouton between 0 h and 72 h
(Number)
Control (toxin)
TeTxLC
iGluR^WT
iGluR^MUT
Control (cpx)
cpx -/-
ns
Control (toxin) UAS-TeTxLC
iGluR^WT iGluR^MUT
Control (cpx) cpx -/-
Bouton Expansion
Formed between 24h to 72h
Formed between 48h to 72h
(% to Initial size)
(hrs)
C
D
E
F
G
H
***
I
J
Bouton Elimination
(%)

Figure S6

Figure S6. Time-lapse images and measurement of bouton formation, expansion and elimination, Related to Figure 5.

A, Representative time-lapse images of synaptic boutons from control [*Vglut-lexA,LexOp-CD8-GFP*/+] at muscles 1/9 labeled with membrane tagged GFP expressed in all MNs. Arrows indicate new immature boutons formed between 0h-24h (white) or 24h-48h (yellow). **B**, Quantification of the number of new boutons added from terminal boutons (n≥26 terminal boutons from n≥7 NMJs) for indicated genotypes. **C-H**, Quantification of the bouton size expansion during time-lapse imaging period (n≥41 boutons from n≥7 NMJs for C-E, n≥18 boutons from n≥7 NMJs for F-H) for indicated genotypes. Imaging period is from 24h to 72h for C-E and from 48h to 72h for F-H. All data are normalized to initial bouton size. **I**, Representative time-lapse synaptic boutons of control [*Vglut-lexA,LexOp-CD8-GFP*/+] at muscle 1/9 labeled with membrane tagged GFP expressed at all MNs. Arrows indicate an eliminated bouton. **J,** Quantification of the percentage of bouton elimination for indicated genotypes (n≥113 of all boutons from n≥7 NMJs). Elimination was scored as the disappearance of bouton between imaging periods. These events are likely not analogous to synaptic 'retractions' as among 113 boutons imaged in control animals we confirmed only a single synaptic 'foot-print' (Dlg staining without presynaptic HRP marker). Scale is the same for images in A and I. For (J), p value was calculated by Fisher's exact test between mutant and control. All error bars indicate ± s.e.m. * =p<0.05, ***=p< 0.001.

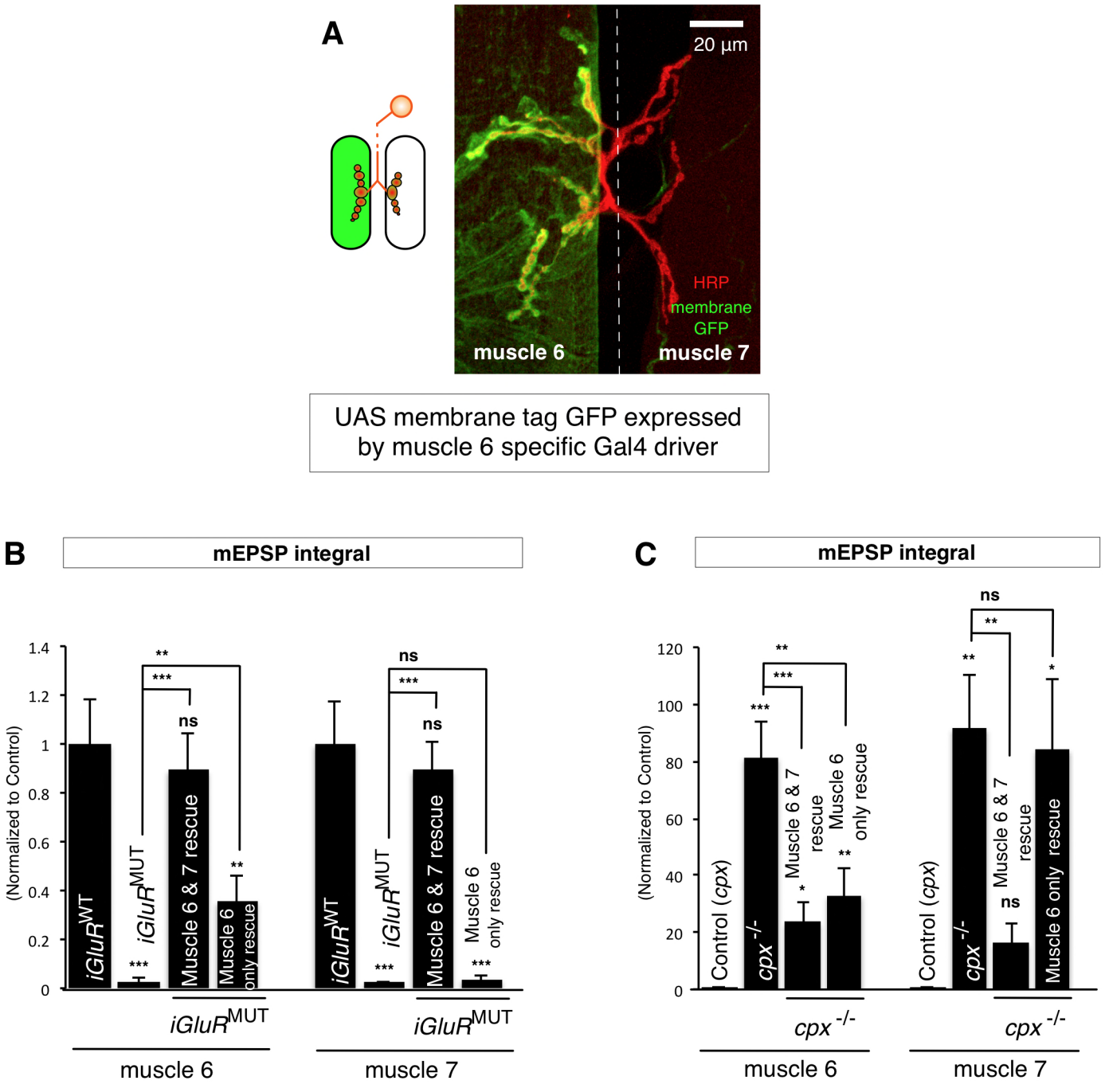
A
20 µm
HRP
membrane
GFP
muscle 6
muscle 7
UAS membrane tag GFP expressed
by muscle 6 specific Gal4 driver
B
mEPSP integral
(Normalized to Control)
iGluR^WT
iGluR^MUT
Muscle 6 & 7 rescue
Muscle 6 only rescue
iGluR^MUT
muscle 6
muscle 7
C
mEPSP integral
(Normalized to Control)
Control (cpx)
cpx -/-
Muscle 6 & 7 rescue
Muscle 6 only rescue
cpx -/-
muscle 6
muscle 7

Figure S7

Figure S7. Representative Muscle 6 specific Gal4 image and electrophysiological quantification, Related to Figure 7.

A, Representative RP3 terminals at muscle 6 and muscle 7, segment A3 from late third instar larvae stage animals labeled with membrane tagged GFP (Green) and neuronal membrane marker HRP (red). UAS-CD8-GFP was expressed with the muscle 6 specific Gal4 driver combination H94-Gal4,nSyb-Gal80 combined with tub^{P}>stop>Gal4, UAS-FLP. The tub^{P}>stop>Gal4 construct was used to demonstrate that the H94-Gal4,nSyb-Gal80 combination does not produce Gal4 in muscle 7 throughout experimental period. **B,C**, Quantification of the mEPSP integral for indicated genotypes ($n \geq 8$ for B, $n \geq 5$ for C).

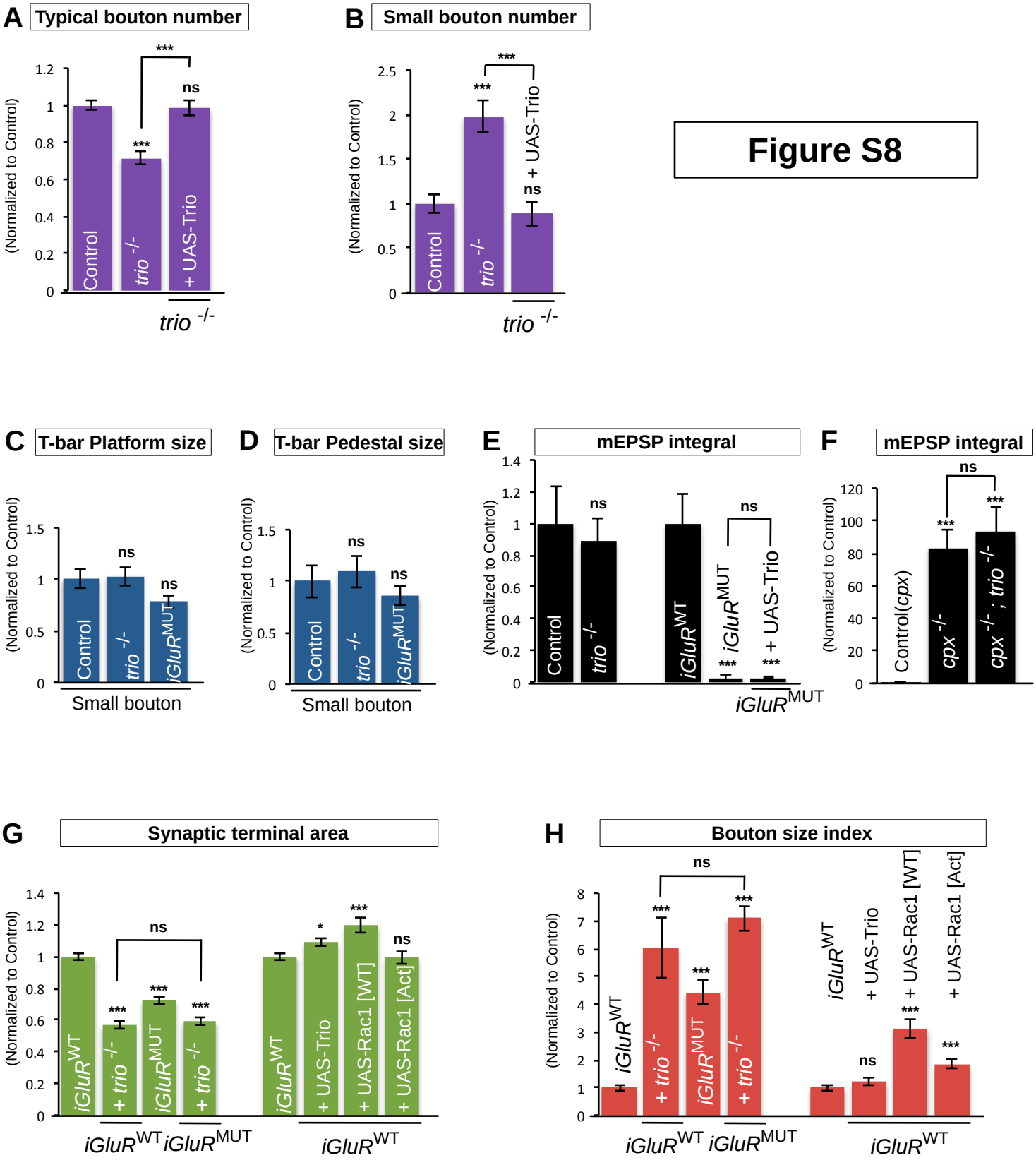
A
Typical bouton number
(Normalized to Control)
Control
trio -/-
+ UAS-Trio
trio -/-
B
Small bouton number
(Normalized to Control)
Control
trio -/-
+ UAS-Trio
trio -/-
Figure S8
C
T-bar Platform size
(Normalized to Control)
Control
trio -/-
iGluRMUT
Small bouton
D
T-bar Pedestal size
(Normalized to Control)
Control
trio -/-
iGluRMUT
Small bouton
E
mEPSP integral
(Normalized to Control)
Control
trio -/-
iGluRWT
iGluRMUT
+ UAS-Trio
iGluRMUT
F
mEPSP integral
(Normalized to Control)
Control(cpx)
cpx -/-
cpx -/- ; trio -/-
G
Synaptic terminal area
(Normalized to Control)
iGluRWT
+ trio -/-
iGluRMUT
+ trio -/-
iGluRWT
+ UAS-Trio
+ UAS-Rac1 [WT]
+ UAS-Rac1 [Act]
iGluRWT iGluRMUT
iGluRWT
H
Bouton size index
(Normalized to Control)
iGluRWT
+ trio -/-
iGluRMUT
+ trio -/-
iGluRWT
+ UAS-Trio
+ UAS-Rac1 [WT]
+ UAS-Rac1 [Act]
iGluRWT iGluRMUT
iGluRWT

Figure S8. Electrophysiological and morphological quantification, Related to Figure 8.

A,B,G,H, Quantification of NMJs including (A) typical bouton number, (B) small bouton number, (G) synaptic terminal area and (H) the bouton size index for indicated genotypes (n≥23 for A,B and n≥22 for G,H). **C,D**, Quantification of the size of T-bar of small bouton from control [CS], *trio* $^{-/-}$ mutant and *iGluR* ^{MUT} mutant (n≥10). **E,F,** Quantification of the mEPSP integral for indicated genotypes (n≥10 for E and n≥8 for F). Control is [CS] (for A-E) and [*cpx*$^{Df/+}$] (for F). All quantification data are normalized to control. Detailed description of used genetypes are followed, Control [CS], Control(*cpx*) [*cpx*$^{Df/+}$], ***trio*$^{-/-}$** mutant [*trio*$^{-/-}$], ***trio*$^{-/-}$ + UAS-Trio** [*UAS-Trio/+;+/OK319-Gal4;trio*$^{-/-}$], ***iGluR*^{WT}** [*dglurIIA*$^{Hypo/-}$*,IIB*$^{Df/-}$*;+/genomic-dglurIIA*^{WT}], ***iGluR*^{MUT}** [*dglurIIA*$^{Hypo/-}$*,IIB*$^{Df/-}$*;+/genomic-dglurIIA*^{E783A}], ***iGluR*^{WT} + *trio*$^{-/-}$** [*dglurIIA*$^{Hypo/-}$*,IIB*$^{Df/-}$*; trio*$^{-/-}$*,genomic-dglurIIA*^{WT}], ***iGluR*^{MUT} + *trio*$^{-/-}$**[*dglurIIA*$^{Hypo/-}$*,IIB*$^{Df/-}$*; trio*$^{-/-}$*,genomic-dglurIIA*^{E783A}], ***iGluR*^{WT} + UAS-Trio** [*dglurIIA*$^{Hypo/-}$*,IIB*$^{Df/-}$*,OK319-Gal4;UAS-Trio/genomic-dglurIIA*^{WT}], ***iGluR*^{WT} + UAS-Rac1^{WT}** [*dglurIIA*$^{Hypo/-}$*,IIB*$^{Df/-}$*,OK319-Gal4;UAS-Rac1*^{WT}*/genomic-dglurIIA*^{WT}] and ***iGluR*^{WT} + UAS-Rac1^{Act}** [*dglurIIA*$^{Hypo/-}$*,IIB*$^{Df/-}$*,OK319-Gal4;UAS-Rac1*^{V12}*/genomic-dglurIIA*^{WT}]. All error bars indicate ± s.e.m. * =p<0.05, **= p<0.01, ***=p< 0.001.

Supplemental Methods

Genetics

The following Gal4 stocks were used: ***OK319-Gal4*** (Beck et al., 2012). OK319-Gal4 is expressed only in the ISN subset of motor neurons (MNs) that includes the motor neurons innervating muscle 4 (morphological analysis), muscles 6 & 7 (morphological & electrophysiological analysis) and muscles 1 & 9 (time-lapse live imaging) beginning in late embryos and continuing throughout larval development until pupation, ***OK6-Gal4*** - Expressed in all larval MNs from late embryos to pupation (Aberle et al., 2002), ***D42-Gal4*** - Expressed in all larval MNs (Yeh et al., 1995), ***G14-Gal4*** - Expressed in larval muscles including muscle 4, 6 and 7 (Aberle et al., 2002), ***C57-Gal4*** - Expressed in larval muscles including muscle 4, 6 and 7 (Budnik et al., 1996), ***H94-Gal4,nSyb-Gal80*** – Expressed in subset of larval muscles including muscles 6 but not muscle 7 (Davis and Goodman, 1998; Rubinstein et al., 2010). Specificity throughout development was confirmed by crossing with *tub^{P}>stop>Gal4, UAS-FLP, UAS-CD8-GFP* (Figure S7A) (Roy et al., 2007).

The following existing transgenic stocks were used: **UAS-TeTxLC** [TNTE] (Sweeney et al., 1995), **UAS-Vglut-RNAi** (UAS-Vglut-RNAi^{JF}, JF02689, target 1278-1724nt of *vglut* transcript) (Figure 1,S1), (UAS-Vglut-RNAi^{HMS}, HMS02011, target 3077-3098nt), (Ni et al., 2008) (Figure S1) or (UAS-Vglut-RNAi^{KK}, VDRC104324, target 1279-1900nt) (Dietzl et al., 2007), (Figure 1,4,S1,S5), **UAS-Vglut** (Daniels et al., 2004), **genomic-*dglurIIA*^{WT}** (DiAntonio et al., 1999), **genomic-*dglurIIA*Δ3UTR** (Schmid et al., 2006), **genomic-*dglurIIA*^{E783A}** (Schmid et al., 2006), **UAS-CamKII^{Act}** (UAS-CamKII^{T287D}) (Haghighi et al., 2003), **UAS-CamKII^{Inh}** (UAS-CamKIINtide) (Haghighi et al., 2003), **UAS-Cpx** (Huntwork and Littleton, 2007), **Vglut-LexA** (Baek et al.,

2013), **LexOp-CD8-GFP** (Baek et al., 2013), **UAS-Trio** (Bateman et al., 2000), **UAS-Rac1^{WT}** (Luo et al., 1994), **UAS-Rac1^{Act}** (UAS-Rac1^{V12}) (Luo et al., 1994).

The following mutant allele stocks were used: ***dglurIIA^{-},B^{-}*** *(dglurIIA,B^{sp22} = dglurIIA and dglurIIB* double null mutant)(DiAntonio et al., 1999), ***dglurIIA^{Df},B^{Df}*** (*Df(2L)cl^{h4}* = deficiency covering both *dglurIIA and dglurIIB*) (DiAntonio et al., 1999)**,** ***dglurIIA^{Hypo},B^{Df}*** (*Df(2L)cl^{h4}*,genomic-*dglurIIA*Δ3UTR), ***vglut^{Hypo}*** (***vglut^{1}*** = *vglut* hypomorphic allele) (Daniels et al., 2006), ***vglut^{Df}*** (*vglut^{OK371ΔD}* = small deficiency covering *vglut*) (Mahr and Aberle, 2006), ***cpx^{-}*** (*cpx^{SH1}* = *cpx* null allele) (Huntwork and Littleton, 2007), ***cpx^{1257}*** (Iyer et al., 2013), ***cpx^{Df}*** (*Df(3R)ED5021* = deficiency covering *cpx*) (Huntwork and Littleton, 2007), ***trio^{-}*** (*trio^{S137203}* = *trio* null allele) (Bateman et al., 2000).

The following allelic combinations were used (DiAntonio et al., 1999; Schmid et al., 2006; Steinert et al., 2006): **CS**: CantonS, ***dgluRIIA$^{+/-}$,IIB$^{-/Df}$*** (Control in Figure 2)**:** *dglurIIA,B^{sp22}/Df(2L)cl^{h4}*;+/genomic-*dglurIIA^{WT}*, ***dgluRIIA$^{Hypo/-}$,IIB$^{-/Df}$:*** *dglurIIA,B^{sp22}/Df(2L)cl^{h4}*,genomic-*dglurIIA*Δ3UTR, ***iGluR^{WT}:*** *dglurIIA,B^{sp22}/Df(2L)cl^{h4}*,genomic-*dglurIIA*Δ3UTR;+/genomic-*dglurIIA^{WT}*, ***iGluR^{MUT}***: *dglurIIA,B^{sp22}/Df(2L)cl^{h4}*,genomic-*dglurIIA*Δ3UTR;+/genomic-*dglurIIA^{E783A}*, **Control (*vglut*) or *vglut$^{Df/+}$***: *vglut^{OK371ΔD}*/+, ***vglut^{MN}***: *vglut^{1}*,*UAS-Vglut-vRNAi^{VDRC104324}*/ *vglut^{OK371ΔD}*;*D42-Gal4*/*UAS-Vglut-RNAi^{JF02689}*, **Vglut-RNAi#1**: *UAS-Vglut-RNAi^{VDRC104324}/+;UAS-Vglut-RNAi^{JF02689}/D42-Gal4*, **Vglut-RNAi#2**: *OK6-Gal4/+;D42-Gal4/UAS-Vglut-RNAi^{HMS},* ***vglut$^{Hypo/Df}$*** : *vglut^{1}/vglut^{OK371ΔD}* **,Control (*cpx*) or *cpx$^{Df/+}$***: *Df(3R)ED5021*/+, ***cpx$^{-/-}$:*** *Df(3R)ED5021*/*cpx^{SH1}*, ***cpx$^{1257/-}$:*** *Df(3R)ED5021*/*cpx^{1257}* , , ***trio$^{-/-}$:*** *trio^{S137203}*/ *trio^{S137203}*. Controls used for each genotype are in figure legends and/or Table S1.

Molecular Biology.

The following transgenes were constructed:

UAS-dGluR^{WT} – Full length *dglurIIA* cDNA.

UAS-dGluR^{DN} –*dglurIIA* cDNA with Glutamic acid at position 783 to mutated to Alanine. This mutation results in a receptor that is correctly localized but non-functional (Schmid et al., 2006).

UAS-rGluK2 – Full length rat GluK2 cDNA (gift from Dr. R.E. Oswald, Cornell University, Ithaca, NY).

UAS-PLTXII and **UAS-δACTX**. – These membrane-tethered toxins are expressed as chimeric fusion proteins comprising (from N to C termini), the secretory signal sequence from Lynx1, native mammalian prototoxin, mature cleaved peptide toxin sequence, glycine-asparagine repeat hydrophilic linker and the Lynx1 GPI targeting sequence (Wu et al., 2008). The complete amino sequence for both toxin peptides are

PLTXII:

MSALLILALVGAAVAADCSATGDTCDHTKKCCDDCYTCRCGTPWGANCRCDYYKARCDTGNG
NGNGNGEQKLISEEDlgNGNGNGNGNGNGNGDGNGGALCNGAGFATPVTLALVPALLATFWS
LL*

δACTX:

MSALLILALVGAAVACAKKRNWCGKTEDCCCPMKCVYAWYNEQGSCQSTISALWKKCGNGN
GNGNGEQKLISEEDlgNGNGNGNGNGNGNGDGNGGALCNGAGFATPVTLALVPALLATFWSLL
*

dGluR^{WT}, dGluR^{DN} and rGluK2 were cloned into pBID-UAS-G and transgenes generated using Phi3C1 site-directed transgenesis (Wang et al., 2012). PLTXII and δACTX were cloned into pUAST (Brand and Perrimon, 1993) and transgenes generated using conventional P-element transgenesis.

Electrophysiology

Intracellular recordings from muscle 6, segment A3 or A4 were performed as previously described (Imlach and McCabe, 2009; McCabe et al., 2003) except for Figure S7 where muscle 6 or 7, segment A3 was used. Briefly, third instar larvae were dissected (0.1mM Ca^{2+}) and recordings carried out in HL3 saline containing 1.5mM Ca^{2+} (physiologically relevant Ca^{2+} concentration). Data was only analyzed from recordings where the resting membrane potential was less than –55 mV. Recordings were performed using an Axoclamp 2B amplifier. Data were low-pass filtered at 1 kHz, digitized, and recorded to disk using a Digidata 1322A interface. eEPSPs, mEPSPs amplitudes, frequency and integrals were measured using the peak detection feature of MiniAnalysis program (Synaptosoft, Inc.). For early first instar larvae recordings, larvae were dissected (0.1mM Ca^{2+}) and recorded in HL3 saline containing 1.0 mM Ca^{2+}. Muscle 6 was whole-cell voltage clamped and mini EPSCs were recorded for 2 min at a holding potential of -80mV. eEPSCs were evoked by stimulating the appropriate segmental nerve with a pulse of 5-8 V that lasted 1ms using a suction electrode. Recordings were made using a Multiclamp 700B amplifier controlled by pClamp 10.2 (Molecular Devices, Sunnyvale, CA). Sampling frequency was 20kHz and traces were filtered at 10kHZ. Data was analysed in Clampfit 10.2, mEPSCs were detected semi-automatic and amplitudes were measured using the event detection tool. **Quantal content** was calculated for each individual recording by calculating (eEPSP amplitude / mEPSP amplitude) (Frank et al., 2006) after correction for nonlinear summation errors (Martin, 1955).

Immunohistochemistry

Wandering third instar larva of comparable size were collected, dissected, and stained as previously described (Brent et al., 2009a; Brent et al., 2009b; McCabe et al., 2003). Briefly,

animals were dissected in 1x PBS (Mediatech) and fixed for 20 minutes in 4% formaldehyde (Sigma-Aldrich). Animals were washed multiple times in PBT (PBS + 0.1% Triton) and then blocked in PBTB (PBT + 0.2% BSA) and PBTN (PBTB+ 2% Normal Goat Serum). Primary antibodies used were mouse anti-Dlg (1:500; Developmental Studies Hybridoma Bank (DSHB) at the University of Iowa), mouse anti-Brp (Wagh et al., 2006) (Nc82, 1:100; DSHB), mouse anti-FasII (1D4, 1:500; DSHB), rabbit anti-Syt1 (1:1000, gift from Troy Littleton, M.I.T., Cambridge, MA), rabbit anti-GluR6/GluK2 (1:1000, Millipore) and rabbit anti-DGluRIII/IIC (Marrus et al., 2004) (1:500, gift from Aaron DiAntonio, Washington University, Saint Louis, MO). Animals were incubated overnight at 4^{o}C in primary antibodies, washed in PBTB and PBTN, and then incubated in secondary antibodies for 2 hours at room temperature. Secondary antibodies used included goat anti-mouse Alexa-488 (1:1000; Invitrogen), goat anti-rabbit Alexa-555 (1:1000; Invitrogen), goat aniti-mouse Cy3 (1:1000; Jackson ImmunoResearch) and Cy5 conjugated HRP (1:400; Jackson ImmunoResearch). Imaging was carried out on Zeiss 510 confocal microscope. To compare intensity levels, experimental and control animals were stained in the same tube and imaged using identical confocal settings and then a maximum projection rendering of z-stacks was analyzed for signal intensity using MetaMorph software (Molecular Devices, Downingtown, PA). Synaptic area was identified by HRP. Intensity was normalized against HRP. For Figure S1D, **the relative frequency histogram of the distribution of bouton sizes**, boundaries of individual boutons were identified manually while blinded to genotype, by using round regional tool of MetaMorph software.

Time-lapse live imaging

Presynaptic motor neurons were labeled with membrane localized LexOp-CD8-GFP expressed by vglut-LexA in both control and mutant backgrounds. All glutamatergic neurons including all type I motor neurons were labeled. Animals were anesthetized by ~15 minute exposure to a

vapor mixture of 35% Methyl Salicylate and 16% Menthol (Haw Par Healthcare Ltd., Singapore) every 24 hours from the second instar onwards for 4 days. For imaging, larva were placed on a slide with 70% glycerol and cover slip. Imaging time was limited to less than 30 minutes after which animals were washed gently with PBS, allowed to recover and returned to the food media. Mutants and corresponding controls were imaged on the same day in a random order to minimize handling variability. For each time point, confocal images (63x, oil immersion lens) of an NMJ terminal z-stack were captured. Type Ib NMJ terminal on muscle 1 or 9 of segment A3 to A6 were chosen for imaging due to exterior localization of these NMJs in muscle field and labeling by the OK319-Gal4 driver. After time-lapse imaging was complete, each animal was dissected, fixed and stained by HRP and Dlg to confirm bouton type. Only images from animals that survived the entire 4-day imaging procedure were included in analysis. For **bouton size expansion in live images**, the size of each bouton was measured using the round regional tool of MetaMorph software while blinded to genotype. Only initial sizes smaller than $2\mu m^2$ (categorized as small bouton) were subjected for analysis throughout imaging period. For **the bouton formation in live images**, only most distal bouton was used for analysis which can be reliably recognized in live imaging. The number of new boutons added between 0h to 72h were counted. For **bouton elimination**, the number of boutons that were lost during 24h to 72h were counted. No bouton re-appeared once eliminated during the imaging period.

Electron microscopy

Fillets from third instar larvae were dissected in HL3 without Ca^{2+} (Jiao et al., 2010a; Jiao et al., 2010b; McCabe et al., 2003). Fillets were then incubated in HL3 buffer containing EDTA for 10 min for resting conditions. The specimens were fixed in 3% glutaraldehyde and 0.5% paraformaldehyde in PBS (pH 7.2) overnight in cold room. Fillets were washed with PBS and postfixed in 1% OsO4, dehydrated in alcohol, and embedded in Durcupan ACM (Fluka). Serial

ultrathin sections were cut with a diamond knife (Diatome), collected on grids and stained with 1% uranyl acetate and lead citrate. The grids were then examined with a JEOL 1200 electron microscope. Images were quantified with NIH ImageJ software.

Supplemental References

Aberle, H., Haghighi, A.P., Fetter, R.D., McCabe, B.D., Magalhães, T.R., and Goodman, C.S. (2002). wishful thinking encodes a BMP type II receptor that regulates synaptic growth in Drosophila. Neuron *33*, 545-558.

Baek, M., Enriquez, J., and Mann, R.S. (2013). Dual role for Hox genes and Hox co-factors in conferring leg motoneuron survival and identity in Drosophila. Development *140*, 2027-2038.

Bateman, J., Shu, H., and Van Vactor, D. (2000). The guanine nucleotide exchange factor trio mediates axonal development in the Drosophila embryo. Neuron *26*, 93-106.

Beck, E.S., Gasque, G., Imlach, W.L., Jiao, W., Jiwon Choi, B., Wu, P.-S., Kraushar, M.L., and McCabe, B.D. (2012). Regulation of Fasciclin II and synaptic terminal development by the splicing factor beag. J Neurosci *32*, 7058-7073.

Brand, A.H., and Perrimon, N. (1993). Targeted gene expression as a means of altering cell fates and generating dominant phenotypes. Development *118*, 401-415.

Brent, J., Werner, K., and McCabe, B.D. (2009a). Drosophila larval NMJ immunohistochemistry. Journal of visualized experiments : JoVE, e1108.

Brent, J.R., Werner, K.M., and McCabe, B.D. (2009b). Drosophila larval NMJ dissection. Journal of visualized experiments : JoVE, e1107.

Budnik, V., Koh, Y.H., Guan, B., Hartmann, B., Hough, C., Woods, D., and Gorczyca, M. (1996). Regulation of synapse structure and function by the Drosophila tumor suppressor gene dlg. Neuron *17*, 627-640.

Daniels, R.W., Collins, C.A., Chen, K., Gelfand, M.V., Featherstone, D.E., and DiAntonio, A. (2006). A single vesicular glutamate transporter is sufficient to fill a synaptic vesicle. Neuron *49*, 11-16.

Daniels, R.W., Collins, C.A., Gelfand, M.V., Dant, J., Brooks, E.S., Krantz, D.E., and DiAntonio, A. (2004). Increased expression of the Drosophila vesicular glutamate transporter leads to excess glutamate release and a compensatory decrease in quantal content. J Neurosci *24*, 10466-10474.

Davis, G.W., and Goodman, C.S. (1998). Synapse-specific control of synaptic efficacy at the terminals of a single neuron. Nature *392*, 82-86.

DiAntonio, A., Petersen, S.A., Heckmann, M., and Goodman, C.S. (1999). Glutamate receptor expression regulates quantal size and quantal content at the Drosophila neuromuscular junction. J Neurosci *19*, 3023-3032.

Dietzl, G., Chen, D., Schnorrer, F., Su, K.-C., Barinova, Y., Fellner, M., Gasser, B., Kinsey, K., Oppel, S., Scheiblauer, S*., et al.* (2007). A genome-wide transgenic RNAi library for conditional gene inactivation in Drosophila. Nature *448*, 151-156.

Frank, C.A., Kennedy, M.J., Goold, C.P., Marek, K.W., and Davis, G.W. (2006). Mechanisms underlying the rapid induction and sustained expression of synaptic homeostasis. Neuron *52*, 663-677.

Haghighi, A.P., McCabe, B.D., Fetter, R.D., Palmer, J.E., Hom, S., and Goodman, C.S. (2003). Retrograde control of synaptic transmission by postsynaptic CaMKII at the Drosophila neuromuscular junction. Neuron *39*, 255-267.

Huntwork, S., and Littleton, J.T. (2007). A complexin fusion clamp regulates spontaneous neurotransmitter release and synaptic growth. Nat Neurosci *10*, 1235-1237.

Imlach, W., and McCabe, B.D. (2009). Electrophysiological methods for recording synaptic potentials from the NMJ of Drosophila larvae. Journal of visualized experiments : JoVE, e1109.

Iyer, J., Wahlmark, C.J., Kuser-Ahnert, G.A., and Kawasaki, F. (2013). Molecular mechanisms of COMPLEXIN fusion clamp function in synaptic exocytosis revealed in a new Drosophila mutant. Mol Cell Neurosci *56C*, 244-254.

Jiao, W., Masich, S., Franzén, O., and Shupliakov, O. (2010a). Two pools of vesicles associated with the presynaptic cytosolic projection in Drosophila neuromuscular junctions. J Struct Biol *172*, 389-394.

Jiao, W., Shupliakov, A., and Shupliakov, O. (2010b). A semi-correlative technique for the subcellular localization of proteins in Drosophila synapses. J Neurosci Methods *185*, 273-279.

Luo, L., Liao, Y.J., Jan, L.Y., and Jan, Y.N. (1994). Distinct morphogenetic functions of similar small GTPases: Drosophila Drac1 is involved in axonal outgrowth and myoblast fusion. Genes Dev *8*, 1787-1802.

Mahr, A., and Aberle, H. (2006). The expression pattern of the Drosophila vesicular glutamate transporter: a marker protein for motoneurons and glutamatergic centers in the brain. Gene Expr Patterns *6*, 299-309.

Marrus, S.B., Portman, S.L., Allen, M.J., Moffat, K.G., and DiAntonio, A. (2004). Differential localization of glutamate receptor subunits at the Drosophila neuromuscular junction. J Neurosci *24*, 1406-1415.

Martin, A.R. (1955). A further study of the statistical composition on the end-plate potential. J Physiol (Lond) *130*, 114-122.

McCabe, B.D., Marqués, G., Haghighi, A.P., Fetter, R.D., Crotty, M.L., Haerry, T.E., Goodman, C.S., and O'Connor, M.B. (2003). The BMP homolog Gbb provides a retrograde signal that regulates synaptic growth at the Drosophila neuromuscular junction. Neuron *39*, 241-254.

Ni, J.-Q., Markstein, M., Binari, R., Pfeiffer, B., Liu, L.-P., Villalta, C., Booker, M., Perkins, L., and Perrimon, N. (2008). Vector and parameters for targeted transgenic RNA interference in Drosophila melanogaster. Nat Methods *5*, 49-51.

Roy, B., Singh, A.P., Shetty, C., Chaudhary, V., North, A., Landgraf, M., Vijayraghavan, K., and Rodrigues, V. (2007). Metamorphosis of an identified serotonergic neuron in the Drosophila olfactory system. Neural Dev *2*, 20.

Rubinstein, C.D., Rivlin, P.K., and Hoy, R.R. (2010). Genetic feminization of the thoracic nervous system disrupts courtship song in male Drosophila melanogaster. J Neurogenet *24*, 234-245.

Schmid, A., Qin, G., Wichmann, C., Kittel, R.J., Mertel, S., Fouquet, W., Schmidt, M., Heckmann, M., and Sigrist, S.J. (2006). Non-NMDA-type glutamate receptors are essential for maturation but not for initial assembly of synapses at Drosophila neuromuscular junctions. J Neurosci *26*, 11267-11277.

Steinert, J.R., Kuromi, H., Hellwig, A., Knirr, M., Wyatt, A.W., Kidokoro, Y., and Schuster, C.M. (2006). Experience-dependent formation and recruitment of large vesicles from reserve pool. Neuron *50*, 723-733.

Sweeney, S.T., Broadie, K., Keane, J., Niemann, H., and O'Kane, C.J. (1995). Targeted expression of tetanus toxin light chain in Drosophila specifically eliminates synaptic transmission and causes behavioral defects. Neuron *14*, 341-351.

Wagh, D.A., Rasse, T.M., Asan, E., Hofbauer, A., Schwenkert, I., Dürrbeck, H., Buchner, S., Dabauvalle, M.-C., Schmidt, M., Qin, G.*, et al.* (2006). Bruchpilot, a protein with homology to ELKS/CAST, is required for structural integrity and function of synaptic active zones in Drosophila. Neuron *49*, 833-844.

Wang, J.-W., Beck, E.S., and McCabe, B.D. (2012). A modular toolset for recombination transgenesis and neurogenetic analysis of Drosophila. PLoS ONE *7*, e42102.

Wu, Y., Cao, G., Pavlicek, B., Luo, X., and Nitabach, M.N. (2008). Phase coupling of a circadian neuropeptide with rest/activity rhythms detected using a membrane-tethered spider toxin. PLoS Biol *6*, e273.

Yeh, E., Gustafson, K., and Boulianne, G.L. (1995). Green fluorescent protein as a vital marker and reporter of gene expression in Drosophila. Proc Natl Acad Sci USA *92*, 7036-7040.